Benchmark of quasi-linear models against gyrokinetic single scale simulations in deuterium and tritium plasmas for a JET high beta hybrid discharge

A. Mariani,[1,*] P. Mantica,[1] I. Casiraghi,[2,1] J. Citrin,[3,4] T. Görler,[5] G.M. Staebler,[6] and Eurofusion JET1 contributors[†]

[1]Istituto per la Scienza e Tecnologia dei Plasmi, CNR, via Cozzi 53, 20125 Milano, Italy
[2]Dipartimento di Fisica 'G. Occhialini', Università di Milano-Bicocca, Milano, Italy
[3]DIFFER-Dutch Institute for Fundamental Energy Research, Eindhoven, The Netherlands
[4]Eindhoven University of Technology, Eindhoven, The Netherlands
[5]Max-Planck-Institut für Plasmaphysik, Boltzmannstraße 2, D-85748 Garching, Germany
[6]General Atomics, San Diego, CA 92186-5608, United States of America

(Dated: March 9, 2021)

A benchmark of the reduced quasi-linear models QuaLiKiz and TGLF with GENE gyrokinetic simulations has been performed for parameters corresponding to a JET high performance hybrid pulse in deuterium. Given the importance of the study of such advanced scenarios in view of ITER and DEMO operations, the dependence of the transport on the ion isotope mass has also been assessed, by repeating the benchmark changing the ion isotope to tritium. TGLF agrees better with GENE on the linear spectra and the flux levels. However, concerning the isotope dependence, only QuaLiKiz reproduces the GENE radial trend of a basically gyro-Bohm scaling at inner radii and instead anti-gyro-Bohm at outer radii. The physics effects which are responsible of the anti gyro-Bohm effect in GENE simulations have been singled out.

I. INTRODUCTION

Turbulent transport is a key factor in determining the fusion performance in any magnetic fusion device. Correctly modelling the particle and heat transport due to micro-turbulence driven by microinstabilities is important in order to predict the density and temperature profiles of a reactor and optimise fusion performance. Numerical codes based on gyrokinetic (GK) theory [1] are the most powerful tool available to perform first-principle modelling of such phenomena. Unfortunately, their computational cost is so high that it is not generally possible to use them to predict plasma profiles and their time evolution. Therefore, simplified ('reduced') models using the quasi-linear (QL) paradigm have been developed, which can be used to interpret the experimental results or to design new experiments, supporting the operations of present and future devices. The two most developed QL models are presently QuaLiKiz [2, 3] and TGLF [4, 5]. In order to improve the reliability of 'reduced' models predictions, a sufficient physics detail has to be included, and a great effort by the fusion community is actually devoted to adding physics ingredients to these models and validating them by comparing the results with those obtained running GK nonlinear (NL) simulations, in addition to comparing with available experiments. The QL models can be used within transport codes to evaluate the fluxes, and have shown to successfully reproduce H-mode deuterium (D) baseline scenarios (fully inductive scenarios with standard confinement with respect to H-mode scaling and moderate β = plasma pressure/magnetic pressure)[6–8]. However, some difficulties have been encountered when addressing high β advanced tokamak scenarios [3, 6, 9–14]. One of the understood reasons is the absence in QL models of nonlinear electromagnetic (EM) stabilization mechanisms, as discussed in [15–18]. Work is ongoing to introduce these effects into QL models [19].

Another domain that has not deserved enough attention is the validation of QL models for isotopes different from deuterium. Indeed, experimentally, heavier isotopes have generally been found to have better confinement time and performances than lighter ones [20–23]. This is in contrast with early theoretical predictions based on modelling Ion Temperature Gradient (ITG)-driven turbulence within an adiabatic electrons, electrostatic (ES) approximation in the collisionless regime, which showed a gyro-Bohm (gB) mass scaling (turbulent fluxes $\propto \sqrt{m_i}$, where m_i is the ion mass). Intensive work has been done on JET, in the framework on the upcoming DT campaign [24, 25], and on AUG to investigate the origin of the observed anti-gB mass scaling of confinement with GK simulations [12, 26–28] and extend predictions to ITER [29]. An anti-gB mass scaling, beneficial for high performance fusion operation, has been found also in GK simulations and attributed, depending on the particular considered cases, to different physics ingredients, such as parallel dynamics of nonadiabatic electrons [30, 31], collisions [32], electromagnetic effects [33, 34], E × B flow shear [33, 35] and different impact of fast particles [12, 27]. The realistic evaluation of the impact of the isotope mass on transport thus requires considering all these physics pieces, and the question arises whether the 'reduced' models are equipped with the necessary physics to model the isotope dependence correctly. In fact, much less work is reported regarding validation of QL models vs experiments in different isotopes [12, 36] and in particular the comparison of QL and GK models in different isotopes is little explored [12, 37]. This is a key topic in view of supporting with predictive modelling the design of fusion reactors with deuterium-tritium (T) operation, typically in high β conditions. This motivated the present work, aiming at comparing QL and GK predictions in different isotopes using as reference case a high beta JET Hybrid discharge, which allows to study both the dependencies of turbulent transport on

* Electronic address: alberto.mariani@istp.cnr.it
† See Joffrin et al. 2019 (https://doi.org/10.1088/1741-4326/ab2276) for the Eurofusion JET1 conributors.

the electromagnetic effects due to high β and on the variation of the ion isotope from D to T.

With this aim, in this work we consider the high performance high β JET hybrid pulse 94875 in D, confronting the results obtained using the two models QuaLiKiz and TGLF with the GK GENE code [38, 39]. We stress that here we are not targeting the validation of the QL models vs the experiment, but just the comparison between GK and QL results, in order to evaluate the capability of QL models to reproduce the physics effects contained in the high fidelity GK codes. For this reason, the reference parameters are not the actual experimental ones, but have been taken from the end of a predictive JETTO [40] simulation in D, where the fluxes were computed using QuaLiKiz (here referred to as 'JETTO-QuaLiKiz' simulation), details of which can be found in [41]. In that simulation, the Electron Temperature Gradient (ETG)-driven transport has been neglected, since it was found negligible in the QuaLiKiz simulations with realistic $Z_{\rm eff}$.

Two radii of analysis $\rho_{\rm tor} = 0.36$ and $\rho_{\rm tor} = 0.6$ have been chosen, to test the impact of different physics ingredients such as electromagnetic effects, $\mathrm{E}\times\mathrm{B}$ shear and fast ions (FI), at inner and outer radii. At both radii, the QuaLiKiz and TGLF linear eigenvalues and heat fluxes have been compared with the results of linear and nonlinear GENE simulations. The paper is organised as follows: in section II the reference plasma parameters, together with the simulations settings, are introduced. Section III shows the comparison of the linear eigenvalues spectra between different models, while the nonlinear fluxes are treated in section IV. In particular, following the linear analysis, the nonlinear simulations have been firstly performed considering a D plasma (section IV A), then all has been repeated in T. The comparison of the D and T cases is contained in section IV B. Conclusions are drawn in section V.

II. EXPERIMENTAL CONDITIONS AND SIMULATION PARAMETERS

The profiles of the main common input parameters of QuaLiKiz, TGLF and GENE simulations, taken from the end of the JETTO-QuaLiKiz simulation, are shown in Fig1.

The electron density n_e is shown in Fig.1 (a), while the electron and ion (D) temperatures $T_{e,i}$ are shown in Fig.1 (b). Impurities have been considered as kinetic species in all the simulations. The considered JET pulse is a recent one, therefore it features the ITER-like wall (ILW), thus displaying Be, Ni and W impurities, which have been taken into account in the simulations. The density profiles of the light impurity, i.e. beryllium, as well of the heavy ones, i.e. nickel and tungsten, have been obtained with a constrained multi-diagnostic analysis, as discussed in [41]. They are shown in Fig.1 (c), compared with n_e. In the simulations, the heavy impurities have been merged to compose a single effective species, conserving the effective charge $Z_{\rm eff} = \sum_j Z_j^2 n_j/n_e$ (sum on ion species; $Z_{\rm eff} = 1.6, 1.9$ at the radii of analysis $\rho_{\rm tor} = 0.36$, $\rho_{\rm tor} = 0.6$, respectively) and imposing neutrality both on density and density gradients. Deuterium FI are produced both by Neutral Beam Injection (NBI) and Ion Cyclotron Resonance Heating Radio Frequency (ICRH RF). The FI densities and temperatures are given in Fig.1 (d) and (e) respectively, compared with the corresponding electron quantities. The FI coming from NBI and RF are here considered as a single species, and their temperature distribution is approximated with a Maxwellian. Therefore, given the total (NBI+RF) FI density $n_{\rm FI}$, the associated temperature has been computed as $T_{\rm FI} = 0.5 * (p_{\parallel,\rm FI} + p_{\perp,\rm FI})/n_{\rm FI}$, where $p_{\parallel,\rm FI}$, $p_{\perp,\rm FI}$ and $n_{\rm FI}$ are the total (NBI+RF) longitudinal and perpendicular pressures of FI, according to JETTO definitions. The investigation of the impact of non-Maxwellian anisotropies is beyond the scope of this work. Considering the FI coming from NBI and RF as a single species could result in a oversimplification, but this has been done to facilitate the comparison of gyrokinetic and quasilinear results. For each considered case, the main ion density, together with its gradient, are obtained enforcing neutrality ($n_i = n_e - \sum Z_{\rm imp.} n_{\rm imp.} - n_{FI}$, where 'imp.' stays for impurity). The impurities are supposed in thermal equilibrium with the main ions. FI have been considered in both GENE and TGLF simulations as a kinetic species, while in QuaLiKiz they enter only through the EM mock-up. Finally, in the figure, the two radii of analysis are indicated by vertical dashed lines.

The magnetic equilibrium has been reconstructed with the EFIT equilibrium solver [42, 43], based on magnetic measurements and pressure constraint. The poloidal plots of the considered magnetic surfaces at the two radii of analysis, together with the last closed flux surface (LCFS), are shown in Fig.2 (a).

The elongation κ and the triangularity δ (computed according to [44]), which are equal to $\kappa = 1.21$ and $\delta = 0.03$ at $\rho_{\rm tor} = 0.36$, respectively, increase, as expected, up to $\kappa = 1.31$ and $\delta = 0.08$ at $\rho_{\rm tor} = 0.6$. The safety factor q profile has been obtained using EFIT enforcing a Faraday rotation constraint, which in particular is needed to have a reliable estimate at smaller radii. It is shown in figure Fig.2 (b). In the QL simulations, both Miller [45] and $s-\alpha$ [46] analytic equilibria have been used, since TGLF features Miller geometry while QuaLiKiz uses $s-\alpha$. The analytic equilibria are the ones that best fit the EFIT equilibrium. The same analytic equilibria have also been used in the GENE simulations. Gyrokinetic results obtained with a more realistic Miller analytic equilibrium, accounting shaping effects such as the elongation and triangularity, which is well suited to compare with TGLF, have been confronted with the ones obtained using a simpler $s-\alpha$ model in order to better compare with QuaLiKiz.

In all the NL GENE and TGLF simulations the rotation shear effects due to NBI injection have been taken into account at both radii. In QuaLiKiz simulations only at $\rho_{\rm tor} = 0.6$, since the impact of $E\times B$ stabilisation is neglected in QuaLiKiz for $\rho_{\rm tor} < 0.5$ due to the systematic underprediction of parallel velocity gradient destabilization in that region in the QuaLiKiz model [3]. The considered toroidal angular rotation $\Omega_{\rm tor}$ radial profile, experimentally obtained with the charge exchange recombination spectroscopy (CXRS) and kept fixed during the JETTO-QuaLiKiz run, is shown in Fig.3.

We assume the plasma flow to be purely toroidal and iden-

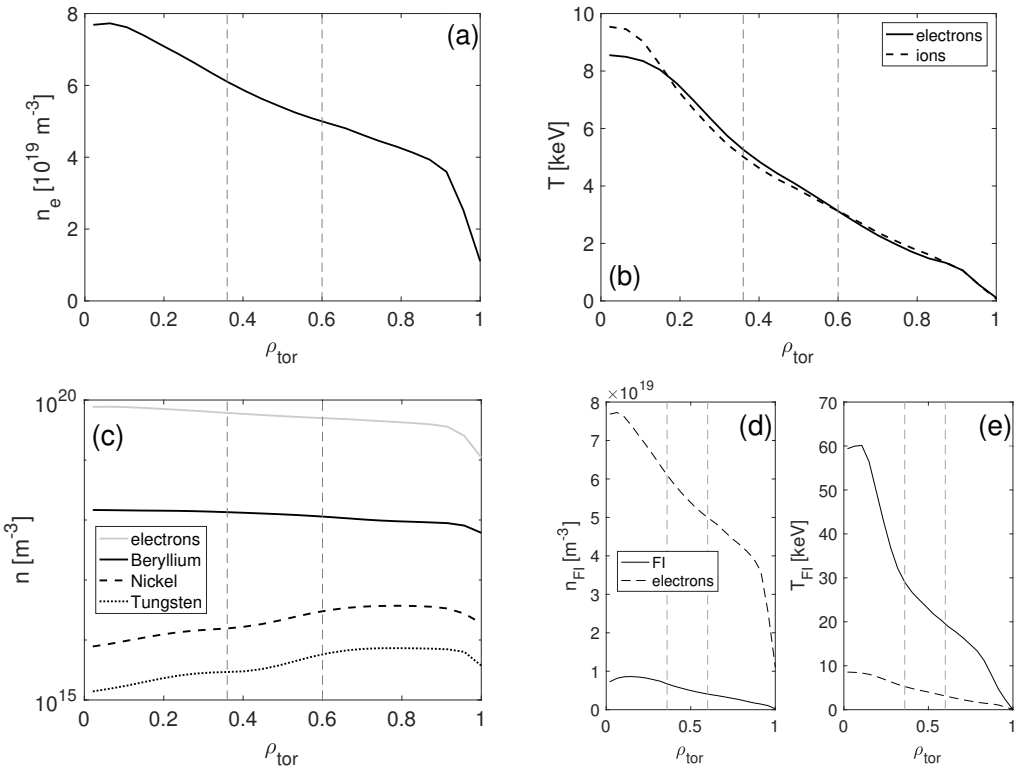

Figure 1. Main plasma parameters at the end of the JETTO-QuaLiKiz simulation (the vertical lines indicate the two radii of analysis): (a) electron density. (b) electron and main ion (deuterium) temperatures $T_{e,i}$. (c) impurities density profiles compared with n_e, in lin-log scale. (d) and (e) FI density and temperature profiles, respectively, compared to electrons.

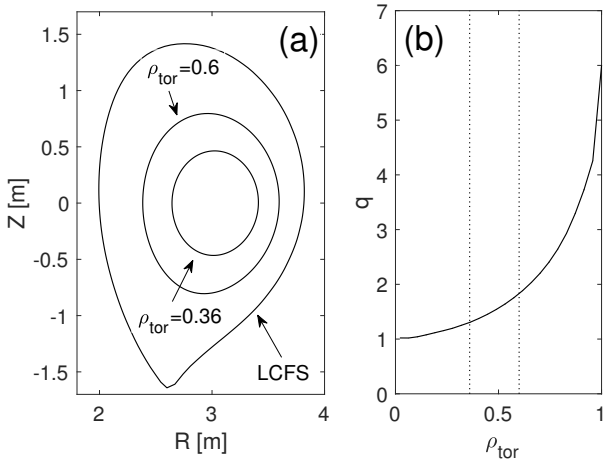

Figure 2. (a) Poloidal plot of the $\rho_{tor} = 0.36, 0.6$ magnetic surfaces, together with the LCFS, obtained using EFIT with pressure constraint. (b) Safety factor profile, obtained using EFIT with Faraday rotation constraint. The vertical lines indicate the radii of analysis.

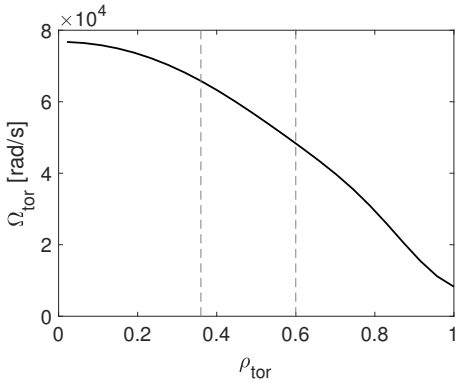

Figure 3. Toroidal angular velocity profile (positive: clockwise as seen from above the tokamak).

tical for all species. Indeed, the contributions to the radial electric field E_r coming from the poloidal and diamagnetic components of the velocity field are small for this case and moreover they almost balance each other. The positive sign in Fig.3 indicates clockwise rotation when viewed from above.

The reference parameters at the two radii of analysis, which are used in the simulations, are collected in Table I.

The normalised radial logarithmic gradients of the f profiles ($f = n, T$) are here defined as $R/L_f = -R\, d\ln f/dr$, where R and r are the plasma major and minor radii at the selected magnetic surface, respectively. The other parameters are the safety factor q, the magnetic shear $\hat{s} = (r/q)dq/dr$, the ratio of the electron plasma pressure to the magnetic pressure $\beta_e = 2\mu_0 n_e T_e/B_0$, with μ_0 the vacuum permeability and $B_0 = 2.72$ T the vacuum magnetic field on the magnetic axis. Finally, the GENE $E \times B$ shearing

El.-ions, q:	R/L_{ne}	R/L_{Te}	R/L_{Ti}	T_i/T_e	q	$\hat{s}$
$\rho_{\rm tor}$ = 0.36	2.97	6.42	6.25	0.95	1.26	0.47
$\rho_{\rm tor}$ = 0.6	2.31	9.93	7.95	1.00	1.83	1.41
Impurities:	n_{Be}/n_e	n_{Ni}/n_e	n_W/n_e	R/L_{nBe}	R/L_{nNi}	R/L_{nW}
$\rho_{\rm tor}$ = 0.36	2.21E-2	2.57E-4	4.81E-5	1.64	-3.73	-1.69
$\rho_{\rm tor}$ = 0.6	2.28E-2	6.02E-4	1.15E-4	3.44	-9.05	-10.82
FI, β_e, E × B:	n_{FI}/n_e	R/L_{nFI}	R/L_{TFI}	T_{FI}/T_e	β_e	$\gamma_E[c_s/R]$
$\rho_{\rm tor}$ = 0.36	0.11	6.24	6.58	5.50	1.75E-2	0.11 (D)
$\rho_{\rm tor}$ = 0.6	0.08	6.84	5.61	6.24	8.49E-3	0.23 (D)

Table I. reference parameters at the end of the JETTO-QuaLiKiz simulation (t = 49.2 s), at the two radii of analysis $\rho_{\rm tor}$ = 0.36 and $\rho_{\rm tor}$ = 0.6, for both D and T simulations. Only γ_E is adapted in T multiplying it by $\sqrt{3/2}$, as explained in the text.

rate $\gamma_E = -(r/q)(\partial\Omega_{\rm tor}/\partial r)R/c_s$ parameter is provided, where $c_s \equiv \sqrt{T_e/m_i}$ is the ion sound speed. The parallel flow shear γ_p was computed consistently with the pure toroidal flow assumption [$\gamma_p \simeq (q/\epsilon)\gamma_E$, where $\epsilon = r/R$ is the inverse aspect ratio]. The $E \times B$ shearing has been turned on at $t = 40R/c_s$ in all the GENE simulations, in order to allow the turbulence to develop before adding its effect. We recall that in GENE the parallel flow shear is active from the beginning of the simulations when set, therefore the initial fluxes overshoot can be enhanced by its presence, because during the overshoot the parallel flow shear is not balanced by the $E \times B$ shearing. The same rotation parameters in physical units have been considered for D and T cases. Therefore, since γ_E scales as $\propto \sqrt{m_i}$, we enforced $\gamma_E(T) = \sqrt{3/2}\,\gamma_E(D)$.

Unless explicitly stated, all the simulations are run in the collisional regime. Since the electron-ion collision rate depends on n_i , which is modified depending on the number of considered species (n_i is adapted using neutrality), the GENE collision parameter $\nu_c = 2.3031 \times 10^{-5} \ln\Lambda\ R[m]n_e[10^{19}m^{-3}]/T_e[keV]^2$ is given in its place, since it only depends on n_e, T_e, where $\ln\Lambda = 24 - \ln(\sqrt{10^{13}n_e[10^{19}m^{-3}]}/10^3 T_e[keV])$ is the Coulomb logarithm. Its values at $\rho_{\rm tor} = 0.36$ and $\rho_{\rm tor} = 0.6$ are $\nu_c = 2.55 \times 10^{-4}$ and $\nu_c = 5.73 \times 10^{-4}$, respectively. The electron-ion thermal collision rate can be easily evaluated for each case as $\nu_{ei} = 4(n_i/n_e)\sqrt{T_e/m_e}\nu_c/R$.

Now some information about the numerical codes is given. The quasi-linear modelling has been performed using the QuaLiKiz and TGLF codes. QuaLiKiz [1] is a GK ES transport model using shifted-circle geometry ($s - \alpha$). Although QuaLiKiz is only ES, it had been possible to obtain approximate QuaLiKiz fluxes in the EM regime using a mockup, based on ES results. This consists in running a R/L_{Ti} scan of QuaLiKiz simulations in the ES regime and then rescaling R/L_{Ti} multiplying it by the radially local ratio $\beta_{\rm thermal}/\beta_{\rm total}$ of the thermal β and total β values (including FI contribution) [3], where $\beta = 2\mu_0 p/B_0^2$, with μ_0 the vacuum permeability. This serves as a rough proxy for the FI enhanced EM stabilisation in NBI and ICRH driven discharges, such as at JET, where the FI content is correlated with EM stabilisation (which itself is not purely due to fast ions), as discussed in [13].

The trapped gyro-Landau fluid model TGLF [2] has been run with saturation rule SAT1 [5], with option UNITS=CGYRO, which improves the description of geometrical effects and is calibrated to a set of CGYRO nonlinear simulations, as discussed in [47]. We refer to this TGLF version as TGLF SAT1-geo. Compared with the original SAT0 model [48], SAT1 features zonal flow mixing, rather than shearing, as the primary saturation mechanism of both ion and electron scale turbulence, and captures cross-scale coupling and nonlinear upshift of the critical R/L_{Ti}. TGLF does not include nonlinear EM stabilization effects, but it includes linear EM effects.

The gyrokinetic simulations have been performed with the GENE code [3]. GENE adopts the following coordinate system in the reduced GK 5-dimentional phase space: a field-aligned coordinate system (x, y, z) in configuration space and $(v_\parallel, \mu)$ as velocity variables in the reduced 2-dimensional GK velocity space. Here (x, y, z) represent the radial, the binormal and the parallel positions respectively (x =const & y =const define a magnetic field line, while z sets the position along that line), $\mu = mv_\perp^2/2B$ is the magnetic moment and $v_\parallel$ is the parallel velocity. The flux-tube version of the code has been used in this work, where a Fourier representation is used for both the x and y directions. A typical grid size for a linear flux-tube simulation with fixed binormal mode number k_y is $n_{kx}\times n_z \times n_{v\parallel} \times n_\mu = 48\times32\times48\times15$, while a typical NL simulation grid size is $n_{kx}\times n_{ky}\times n_z \times n_{v\parallel} \times n_\mu = 128\times32\times32\times48\times15$. To collect sufficient statistics, the NL flux-tube simulations have been run in time up to at least $t_{\rm max}c_s/R \sim 100$, or up to $t_{\rm max}c_s/R \sim 1000$ when necessary. Convergence tests have been performed to check the reliability of the results. The minimum binormal wavenumber $k_{y,\rm min}\rho_s = 0.05$ has been chosen for both linear scans and NL simulations. The x box size typical value has been set to $L_x = 120\rho_s$, with $\rho_s = c_s/\Omega_i$ the sound Larmor radius and Ω_i the ion cyclotron frequency. Convergence tests have been done down to $k_{y,\rm min}\rho_s = 0.03$ and up to $L_x = 200\rho_s$. EM simulations have been compared with ES ones to single out the impact of the electromagnetic effects on the results. The effect of finite β on the geometry has been retained in the ES simulations, to separate geometrical effects linked to Shafranov shift and the dynamical finite β effects which are associated with magnetic field fluctuations, when comparing with the EM case. This has been done by setting the $\alpha_{\rm MHD} = -q^2 R d\beta/dr$ parameter in ES simulations equal to its value in EM ones, including the FI contribution to β when they have been considered. Collisions have been taken into account unless otherwise stated, through a Landau collision operator.

Given that the FI pressure gradient at $\rho_{\rm tor} = 0.36$ is sufficiently high to destabilise low-k EM modes in linear and nonlinear GK simulations when the EM regime is addressed

[1] Git hash 6a57e45b, which has the same physics characteristics as QuaLiKiz tag 2.7.0

[2] Git hash bf11cdd

[3] GENE release-1.8 (Git hash 99cb22) has been employed

(i.e. finite β_e is considered), leading to unphysical large values of simulated NL turbulent fluxes in GENE runs, we tuned down the FI pressure and density until the linear low-k EM modes disappear. This is indeed physically consistent, since FI-driven modes, once destabilised, would reduce the FI density gradients and density. Therefore, it makes sense to reduce these values until mode stability, as discussed in [15]. Therefore, after performing $R/L_{n,\mathrm{FI}}$ scans of γ for different values of n_{FI}/n_e (varying $R/L_{T,\mathrm{FI}}$ proportionally to $R/L_{n,\mathrm{FI}}$ for simplicity), together with checking that nonlinearly the obtained flux remains finite and reasonable, we identified the minimum required FI pressure change to stabilise the low-k EM modes: n_{FI}/n_e : $0.11 \rightarrow 0.08$, $R/L_{n,\mathrm{FI}}$: $6.24 \rightarrow 5$ and $R/L_{T,\mathrm{FI}}$: $6.58 \rightarrow 5.28$. This corresponds to going from the dashed curve to the solid one in Fig.4 (a), where a GENE k_y scan of the linear growth rate γ at $\rho_{\mathrm{tor}} = 0.36$ in the EM regime is presented.

It can be seen that the linear low-k EM modes are stabilised by varying the FI parameters. This new set of FI parameters has been considered instead of the reference one for all the TGLF and GENE simulations at $\rho_{\mathrm{tor}} = 0.36$. Fig.4 (b) and (c) show β_e scans of γ and ω for the low-k EM peak in Fig.4 (a), varying the FI content. It can be seen that FI strongly affect the instability β_e threshold, and that the chosen FI content corresponds to marginal linear stability. This supports the identification of this EM modes as Beta induced Alfvén Eigenmodes (BAE) [49]. These modes are likely coupled with Kinetic Ballooning Modes (KBM) [50], which are characterised by similar large positive frequencies (following GENE sign conventions), ballooning parity and a β_e threshold. Indeed, these EM modes are destabilised when increasing β_e beyond a threshold (see Fig.4 (b)), they display high positive frequencies (see Fig.4 (c)), and they show ballooning parity, that is $\bar{\phi}(k_y, \bar{z})$ is even, while $\bar{A}_{\parallel}(k_y, \bar{z})$ is odd (this has been tested inspecting $|\bar{\phi}(k_y, \bar{z})|$ and $|\bar{A}_{\parallel}(k_y, \bar{z})|$ at different low values of k_y), where $\bar{\phi}(k_y, \bar{z})$ and $\bar{A}_{\parallel}(k_y, \bar{z})$ represent the complex ballooning representations of the (k_x, k_y) Fourier transforms of the ES potential ϕ and the parallel vector potential $A_{\parallel}$, respectively. The ballooning representation $\bar{\phi}$ is related to the (k_x, k_y) Fourier transform $\hat{\phi}(k_x, k_y, z)$ of ϕ by the relation $\hat{\phi}(k_x = p\Delta k_x, k_y, z) = \bar{\phi}(k_y, \bar{z} = z + p2\pi)$ ($\Delta k_x = 2\pi/L_x$, $L_x = 1/k_y\hat{s}$ being the size of the flux-tube along the x direction for a given linear k_y mode), where $\bar{z}$ indicates the extended ballooning coordinate (the same holds for $A_{\parallel}$). However, a deeper analysis of the nature of these coupled modes is beyond the scope of this work. In the following we will simply refer to this mode as a hybrid BAE/KBM, following [15]. From a further inspection of Fig.4 (a), one notes that the growth rate corresponding to the smallest $k_y\rho_s = 0.05$ is unchanged by the FI content variation. This has been investigated, and the corresponding linear mode has been identified as a micro-tearing mode (MTM). Indeed, it shows negative frequency (according to GENE conventions) and tearing mode parity (odd $\bar{\phi}(k_y, \bar{z})$, even $\bar{A}_{\parallel}(k_y, \bar{z})$). The same holds at the even smaller wavenumber $k_y\rho_s = 0.03$, which has been tested given that $k_y\rho_s = 0.03, 0.05$ are the minimum values of k_y which have been set in the NL simulations.

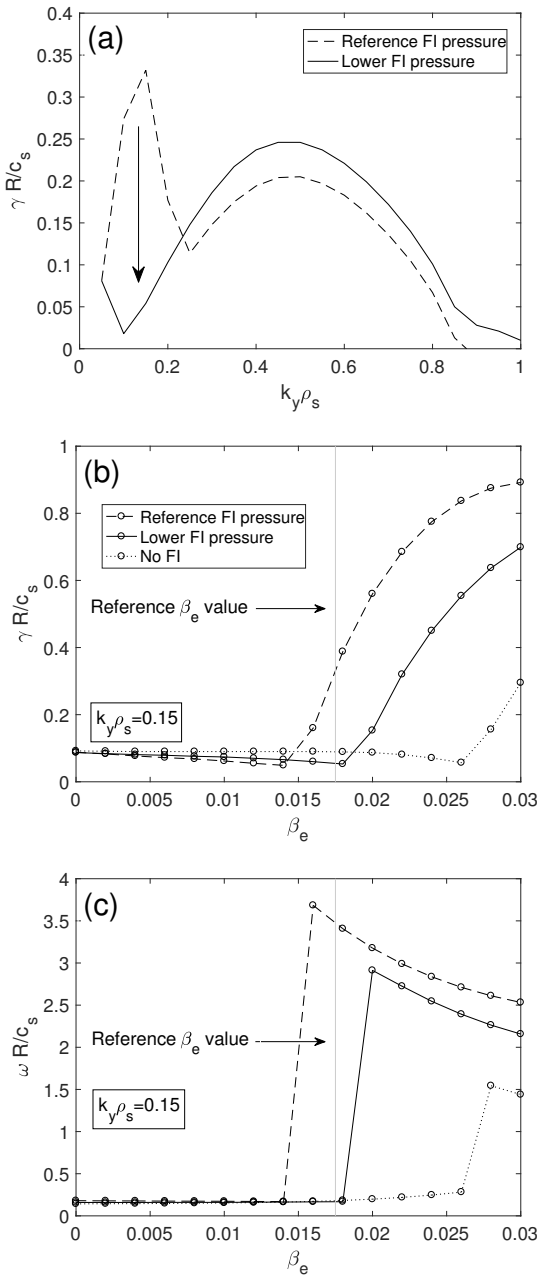

Figure 4. (a) Comparison of k_y spectra of the growth rate γ of the first linear unstable mode at $\rho_{\mathrm{tor}} = 0.36$, comparing the results obtained using the reference FI parameters (end of the JETTO-QuaLiKiz simulation) and reducing FI density and pressure gradient according to n_{FI}/n_e : $0.11 \rightarrow 0.08$, $R/L_{n,\mathrm{FI}}$: $6.24 \rightarrow 5$ and $R/L_{T,\mathrm{FI}}$: $6.58 \rightarrow 5.28$. The latter parameters correspond to the ones used in the GENE/TGLF simulations. (b) and (c) β_e scans of the linear growth rate γ and frequency ω, respectively, for $k_y\rho_s = 0.15$, corresponding to the peak of the EM low-k modes in (a). The two FI content cases of (a) are considered, compared with a third one where the FI are completely removed. Both γ and ω are normalised with c_s/R. The vertical grey line indicates the reference value of. β_e at $\rho_{\mathrm{tor}} = 0.36$ (see table I).

III. LINEAR ANALYSIS

In order to characterise the linear drivers of the microturbulence leading to turbulent fluxes for the selected cases, k_y scans of GENE linear flux-tube simulations in D have been run for the reference parameters of Table I, corresponding to the two radii of analysis. The results obtained with QuaLiKiz and TGLF have then been confronted with GENE, considering both electrostatic (ES) and electromagnetic (EM) regimes, to single out the impact of linear EM stabilisation.

For the GENE-QuaLiKiz comparison, only the ES regime has been addressed, since QuaLiKiz is essentially an ES code. Since QuaLiKiz features $s-\alpha$ geometry, also GENE has been run with this geometry. Finally, FI have not been considered in QuaLiKiz since the possibility of including them in QuaLiKiz standalone runs has not yet been tested sufficiently. Therefore they have been neglected also in GENE when comparing with QuaLiKiz at the inner radius, where the FI content is larger, for consistency. However, as will be shown in section IV, FI have been considered for QuaLiKiz in the flux computation for the EM case using its EM mockup (see section II). TGLF and GENE have been compared in both ES and EM regimes. Since TGLF adopts Miller geometry, that has been set also in GENE. FI have been considered as kinetic species in both codes. As a consequence, the linear EM stabilisation effects have been taken into account in both GENE and TGLF. All the simulations have then been repeated in T. Figures 5 and 6 show the k_y spectra of the growth rate γ and frequency ω of the first unstable linear mode, comparing the QL models QuaLiKiz and TGLF (colors), respectively, with GENE (greyscale), at $\rho_{\rm tor} = 0.36$ (first row) and $\rho_{\rm tor} = 0.6$ (second row).

Let us start from the GENE-QuaLiKiz comparison (Fig.5). Looking at the growth rates (Fig.5 (a) and (c)), QuaLiKiz underestimates them (both peak and the corresponding k_y) at both radii, but at least the agreement with GENE is better for the smallest wavenumbers, which contribute more to the nonlinear fluxes. The frequency spectra (Fig.5 (b) and (d)) show a qualitative QuaLiKiz-GENE agreement on identifying the ion-scale and electron-scale dominant turbulence regimes as ITG and ETG, corresponding to positive and negative frequencies, respectively. In particular, at $\rho_{\rm tor} = 0.36$ the ITG and ETG regimes are separated by a gap, while at $\rho_{\rm tor} = 0.6$ a continuous TEM-ETG branch fills the intermediate region, due to the fact that the 43% larger value of the TEM driver R/L_{Te} at $\rho_{\rm tor} = 0.6$ is not compensated by the larger collisionality and shear values, leading to TEM destabilisation.

Turning to the GENE-TGLF comparison (Fig.6), here both ES and EM cases have been addressed. First, we consider the results obtained using GENE alone, comparing these two regimes. From the inspection of γ vs k_y, a much stronger linear EM stabilisation (grey lines $\rightarrow$ black lines) is seen at the inner radius $\rho_{\rm tor} = 0.36$, compatible with the fact that $\beta_e(\rho_{\rm tor} = 0.36)/\beta_e(\rho_{\rm tor} = 0.6) \sim 2$. To better understand this results, we performed β_e scans of linear GENE simulations at fixed $k_y\rho_s = 0.3$ (roughly corresponding to the peaks of the nonlinear flux spectra, see section IV) for parameters corresponding to the two radii of analysis. The results are shown in Fig.7, where the growth rates are normalised with the ones that are obtained setting $\beta_e = 0$.

It has to be pointed out that in these scans $\alpha_{\rm MHD}$ has been computed self-consistently, therefore the $\beta_e = 0$ results have not to be directly compared with the ones obtained in the other ES simulations, where $\alpha_{\rm MHD}$ has been kept equal to the reference EM value to retain finite β effects on the geometry (see section II) even in the ES case. Figure 7 shows that the much larger linear EM stabilisation effect that is observed at $\rho_{\rm tor} = 0.36$ is due to the concomitance of two reasons: firstly, as it was already stated, β_e is almost twice compared to $\rho_{\rm tor} = 0.6$, secondly the negative slope of $\gamma(\beta_e)/\gamma(\beta_e = 0)$ is much larger at the smaller radius. Coming back to the eigenvalues spectra (Fig.6), the frequencies ω are compatible with ITG and ETG modes at ion- and electron-scales respectively, for both ES and EM cases at both radii. Turning to the isotope comparison, T growth rates are moderately smaller than D ones at the lower wavenumbers which mostly contribute to the fluxes (consider that this difference is a little bit smoothed out in the plots since the γ normalisation c_s/R scales with $1/\sqrt{m_i}$), with the largest difference at $\rho_{\rm tor} = 0.36$ in the EM regime.

Comparing TGLF with GENE, the agreement on the growth rates is very good for the ES case at both radii, better than the GENE-QuaLiKiz one. The agreement is still very good for the EM case at the outer radius, while it is worse for the EM case at the inner radius, while however TGLF for that case agrees with GENE on predicting smaller γ values for T wrt. D. The GENE-TGLF agreement on the frequencies is very good for all the cases.

Since the GENE-QuaLiKiz and GENE-TGLF benchmarks have been performed using different analytic equilibria, a comparison of GENE linear k_y scans of γ varying the geometry from $s-\alpha$ to Miller is presented, at $\rho_{\rm tor} = 0.36$ and $\rho_{\rm tor} = 0.6$, for the common ES case with D isotope, as shown in Fig.8. As expected, the shaping effects are more important at the outer radius, where κ and δ are larger (see section II), and both larger γ peaks and corresponding k_y are observed for Miller equilibrium compared to $s-\alpha$, consistently with [51].

Finally, the ratio $(\gamma/k_y)_{\rm max,ETG}$ of the maximum growth rate for the ETG branch at electron-scales has been confronted with the corresponding value for the ITG branch at ion-scales, in order to test the criterion $[(\gamma/k_y)_{\rm max,ETG}]/[(\gamma/k_y)_{\rm max,ITG}] > 1$ for ETG relevance [52], stating that if this condition holds ETGs should impact the NL fluxes. However, for all the GENE, QuaLiKiz and TGLF simulations which are presented in this section, it has been found $[(\gamma/k_y)_{\rm max,ETG}]/[(\gamma/k_y)_{\rm max,ITG}] \lesssim 50\%$, indicating that ETGs are not expected to cause significant heat transport for the considered cases. This is consistent with the fact that the parameters which have been considered in this work come from a JETTO-QuaLiKiz simulations without ETGs (see the introduction), where $T_e \sim T_i$. In the actual experiment $T_i > T_e$ (although also $T_e \sim T_i$ roughly lies within error bars), corresponding to a more ETG-unstable case, since the ETG R/L_{Te} instability threshold is proportional to $1 + Z_{\rm eff}T_e/T_i$ [53]. A more definitive study of ETG relevance in this JET pulse is shown in a separate related study [41].

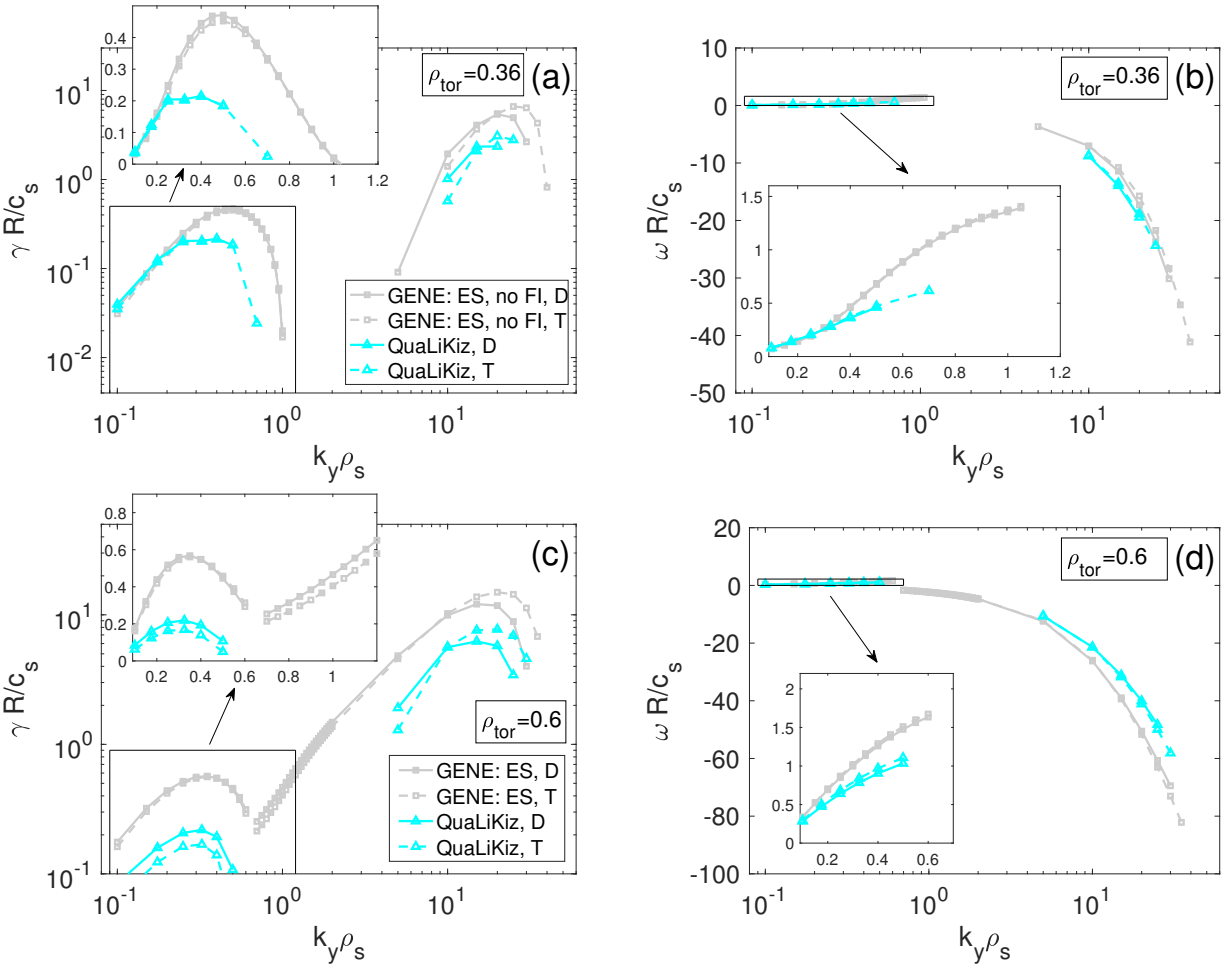

Figure 5. (color online) Comparison of k_y spectra of the growth rate γ (a)/(c) and frequency ω (b)/(d) of the first unstable linear mode, comparing QuaLiKiz with GENE, at $\rho_{\rm tor} = 0.36$ (first row) and $\rho_{\rm tor} = 0.6$ (second row). GENE has been run only in the ES regime with $s-\alpha$ geometry, as well as without FI at the inner radius, to better compare with QuaLiKiz.

IV. NONLINEAR ANALYSIS

QuaLiKiz and TGLF ion and electron heat fluxes have been compared with GENE nonlinear flux-tube ion-scale simulations at the two radii of analysis, considering both D and T cases. Both the ES and EM cases have been accounted for in the GENE-QuaLiKiz benchmark, where the EM mockup has been used for QuaLiKiz in the EM case (see section II). Consistently with the linear analysis (see section III), $s-\alpha$ geometry has been considered also in GENE, to better compare the two codes. For the same reason, FI have been neglected in GENE ES simulations at the inner radius $\rho_{\rm tor} = 0.36$, where the FI content is larger, since QuaLiKiz does not include FI.

Only the EM case has been considered for the GENE-TGLF benchmark, being the most significant one, in order not to repeat all the GENE ES $s-\alpha$ simulations using Miller geometry, since TGLF only runs with the latter. For this case, kinetic FI have been considered in both codes. However, it has to be pointed out that while TGLF retains linear EM stabilisation effects (see section III), it is not able to model NL EM stabilisation, as will be shown.

A. Nonlinear results in deuterium

First, we shall consider D results. R/L_{Ti} scans of the ion and electron heat fluxes $qigB$ and $qegB$ in gyro-Bohm units have been performed, since R/L_{Ti} is the main driver of ITG modes, which have been found to be the principal instability from linear simulations at both radii (see section III). Here, $qgB = q/q_{\rm GB}$, where $q = q_i, q_e$ are the radial ion/electron heat fluxes per unit surface and $q_{\rm GB} = \sqrt{m_i} n_e T_e^{5/2}/e^2 R^2 B_0^2$ is the gyro-Bohm normalisation. The results are shown in Fig.9 (a) and (b), corresponding to $\rho_{\rm tor} = 0.36$ and $\rho_{\rm tor} = 0.6$ respectively.

The fluxes are shown by solid/dashed lines for the ES and EM cases respectively (TGLF results are indicated by dotted lines to distinguish them from QuaLiKiz ones). GENE fluxes are distinguished from QL ones by displaying square markers. The GENE error bars represent the standard deviation of the fluxes time traces over the same time interval that has been considered to compute their averages.

Looking first to GENE alone, the results clearly show a much stronger EM stabilisation at $\rho_{\rm tor} = 0.36$ than at $\rho_{\rm tor} =$

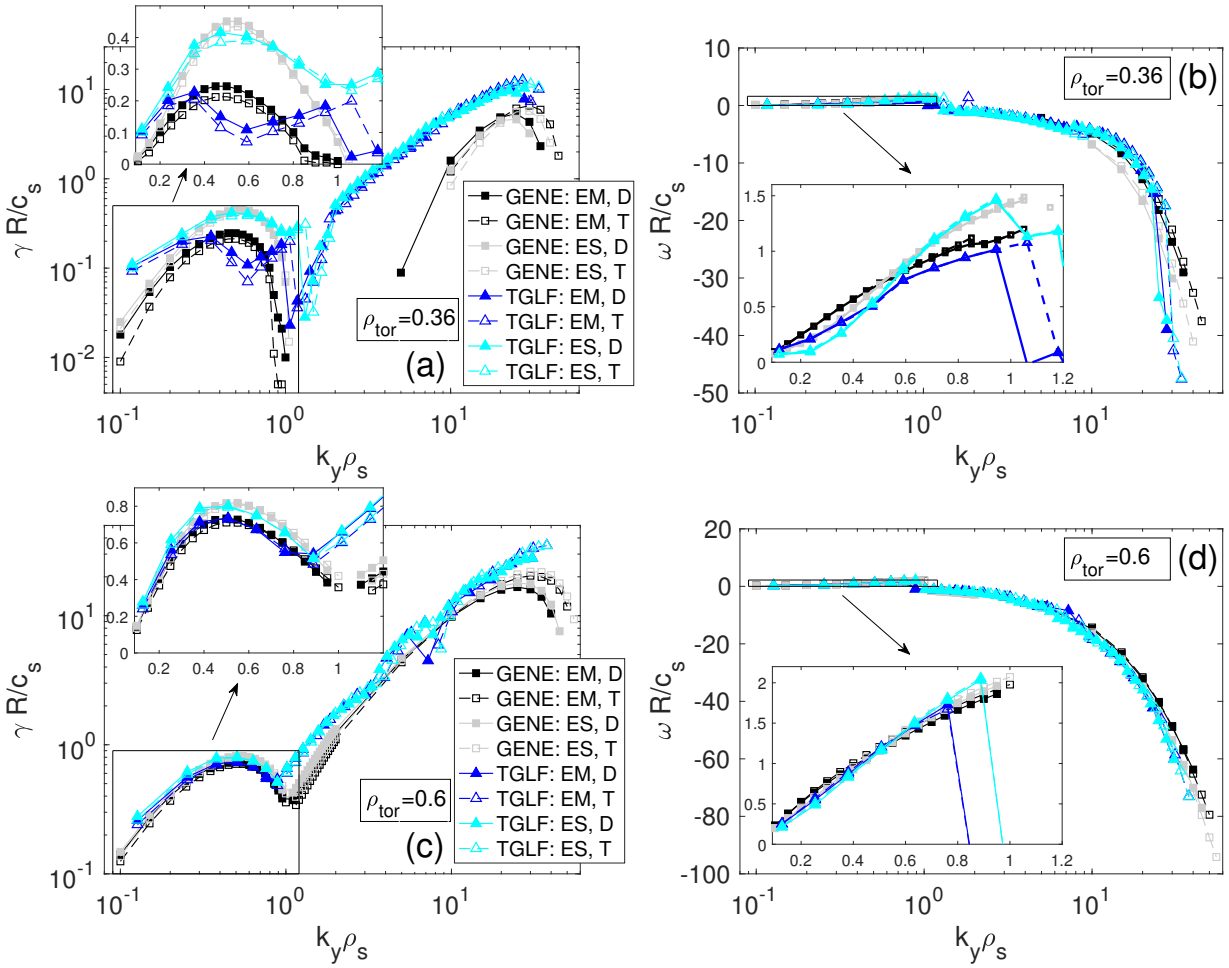

Figure 6. (color online) Comparison of k_y spectra of the growth rate γ (a)/(c) and frequency ω (b)/(d) of the first unstable linear mode, comparing TGLF with GENE, at $\rho_{\rm tor} = 0.36$ (first row) and $\rho_{\rm tor} = 0.6$ (second row).

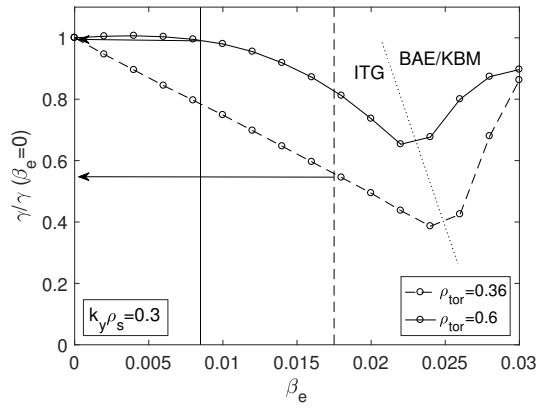

Figure 7. Growth rate γ divided by the value obtained setting $\beta_e = 0$, versus β_e, with $k_y\rho_s = 0.3$, at $\rho_{\rm tor} = 0.36$ (dashed) and $\rho_{\rm tor} = 0.6$ (solid). the vertical lines indicate the β_e value at the two radii, following the same line style.

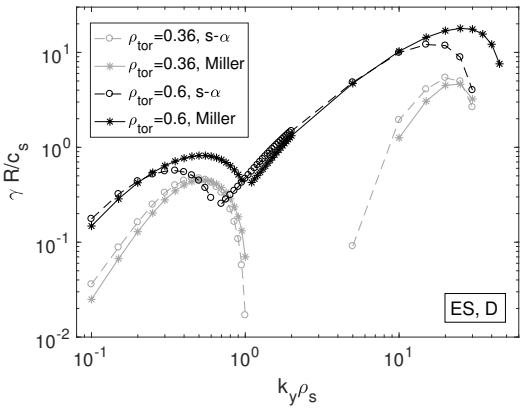

Figure 8. $s-\alpha$ (dashed-circle) vs Miller (solid-asterisk) comparison of GENE linear k_y scans of γ, at $\rho_{\rm tor} = 0.36$ (grey) and $\rho_{\rm tor} = 0.6$ (black). The ES case is considered, with D isotope.

0.6, consistent with linear results. Moreover, considering the EM cases, the fluxes seem not to increase with increasing R/L_{Ti} at both radii. This lack of R/L_{Ti} stiffness has been investigated by performing linear GENE simulations, in order to quantify if a portion of this 'flattening' could be due to a

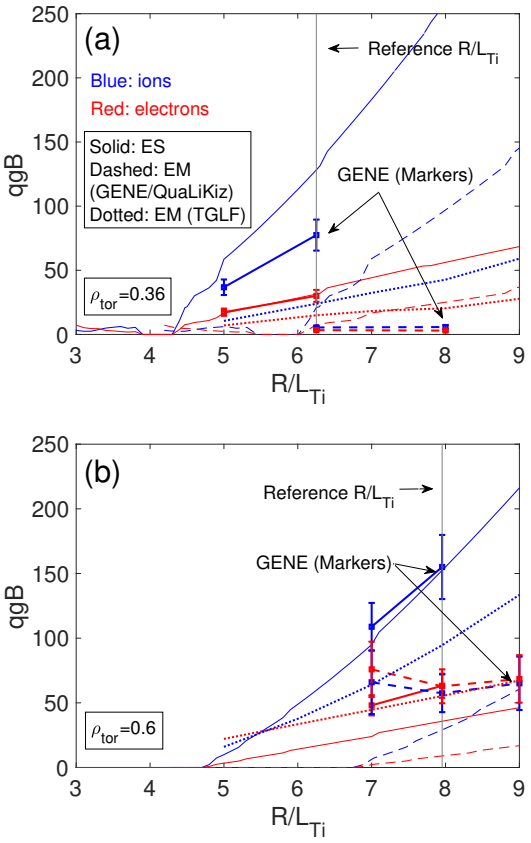

Figure 9. (color online) GENE NL fluxes compared with QuaLiKiz and TGLF QL fluxes in gyro-Bohm units vs R/L_{Ti} in D, comparing QL models with GENE, at $\rho_{\rm tor} = 0.36$ (a) and $\rho_{\rm tor} = 0.6$ (b). Ion and electron heat fluxes are indicated in blue and red, respectively. The ES and EM cases are shown by solid and dashed lines, respectively, except for TGLF in the EM regime, that is indicated by dotted lines to differentiate it from QuaLiKiz. GENE is marked with squares, and the corresponding error bars represent the standard deviation of the fluxes time traces over the same time interval that has been considered to compute their averages.

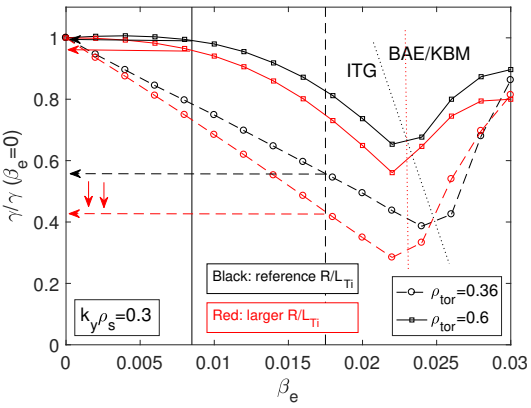

Figure 10. Growth rate γ divided by the value obtained setting $\beta_e = 0$, versus β_e, with $k_y\rho_s = 0.3$, at $\rho_{\rm tor} = 0.36$ (dashed) and $\rho_{\rm tor} = 0.6$ (solid). the vertical lines indicate the β_e value at the two radii, following the same line style. The results corresponding to reference parameters are shown in black, while the ones that have been obtained increasing R/L_{Ti} alone to $R/L_{Ti} = 8$ and $R/L_{Ti} = 9$ at $\rho_{\rm tor} = 0.36$ and $\rho_{\rm tor} = 0.6$, respectively, are indicated by red lines.

more efficient linear β_e stabilisation at larger R/L_{Ti} ('R/L_{Ti} stiffness' means the degree to which the normalised heat flux responds to changes in R/L_{Ti}). To do that, the β_e scans of Fig.7 have been repeated increasing R/L_{Ti} alone by ~ 1, to $R/L_{Ti} = 8$ and $R/L_{Ti} = 9$ at $\rho_{\rm tor} = 0.36$ and $\rho_{\rm tor} = 0.6$, respectively. Indeed, approximating the saturation levels of the NL potentials with a mixing length rule $\sim \gamma/k_\perp^2$, we can at the first order suppose that the linear EM stabilisation of the NL fluxes should roughly be proportional to the γ reduction due to finite β_e. Figure 10 shows the results in red, compared with those obtained at smaller R/L_{Ti}, in black, which correspond to Fig.7.

A $\Delta\gamma \sim -23\%$, -4% reduction is observed at $\rho_{\rm tor} = 0.36$ and $\rho_{\rm tor} = 0.6$, respectively. Moreover, a slight reduction of the BAE/KBM onset β_e threshold is observed with increasing R/L_{Ti}, confirming a larger impact of BAE/KBM EM modes with increasing R/L_{Ti}. These reductions of γ, however, despite they have the right sign to be related to a contribution coming from linear EM stabilisation to the flattening of qgB vs R/L_{Ti}, are not sufficient to fully explain it, as it can be seen looking at Fig.9. The remaining contribution should then come from NL effects.

Finally, GENE predicts $q_e > q_i$ at $\rho_{\rm tor} = 0.6$ for the EM case. This is due to the fact that there is a $\sim 30\%$ EM contribution to q_e, mainly coming from $B_\perp$ fluctuations, that reverses the q_i/q_e ratio in the EM regime at the outer radius. Going in more details, EM contributions to q_e, coming from both perpendicular and parallel B fluctuations, have been neglected in the NL GK simulations at $\rho_{\rm tor} = 0.36$, while they have been retained at $\rho_{\rm tor} = 0.6$. This choice follows the inspection of the NL spectra of the GK fluxes. The NL k_y spectra of the electron flux $qegB(k_y)$ are shown at $\rho_{\rm tor} = 0.36$ and $\rho_{\rm tor} = 0.6$ in Fig.11 (a) and (b), respectively, for the EM case with reference parameters.

Here, $qegB = \sum_{k_y} qegB(k_y)$. The total flux (solid) is split in its ES part, coming from ϕ fluctuations (dotted), and the EM part which comes from both perpendicular and parallel magnetic field fluctuations (dotted). The EM part at $\rho_{\rm tor} = 0.36$ is a $< 20\%$ contribution to a very small $qegB \sim 3$, coming from a spectrum which decays by only ~ 1 order of magnitude within the k_y box, even after collecting a large statistics ($t_{\rm max} \sim 800R/c_s$), therefore it has been neglected. On the contrary, the EM contribution to $qegB$ at $\rho_{\rm tor} = 0.6$ is positive for all k_y values, it decays by ~ 2 orders of magnitudes within the k_y box and contributes $\sim 27\%$ to a non-negligible $qegB \sim 63$ flux. As a consequence it has been retained. The dependence of the fluxes on FI has been also analysed at $\rho_{\rm tor} = 0.36$, where the EM effects are larger. The GENE NL EM simulation with reference parameters has been repeated removing FI, and the results are compared in Fig.12 (a), where the time traces of the fluxes in gyro-Bohm units are shown.

It turns out that the effect of FI on fluxes is negligible. This is possibly due to the fact that the EM NL stabilisation is so

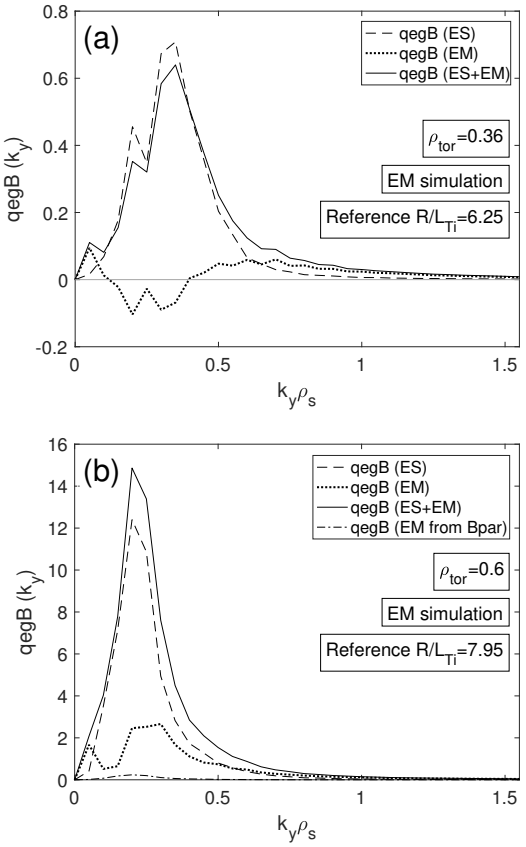

Figure 11. GENE NL flux spectra in gyro-Bohm units, satisfying $qegB = \sum_{k_y} qegB(k_y)$, from the EM simulations at $\rho_{\rm tor} = 0.36$ (a) and $\rho_{\rm tor} = 0.6$ (b), for reference parameters from the JETTO-QuaLiKiz simulation. The total fluxes (solid) are separated in the ES contribution (dashed), coming from ϕ fluctuations, and EM contribution (dotted), coming from $B_\perp$ and $B_{||}$ fluctuations. In (b), the EM contribution coming from only $B_{||}$ fluctuations is also shown by a dashed-dotted line. The two spectra have been obtained averaging the $\Delta t = 680 - 786\ R/c_s$ (a) and $\Delta t = 180 - 272\ R/c_s$ (b).

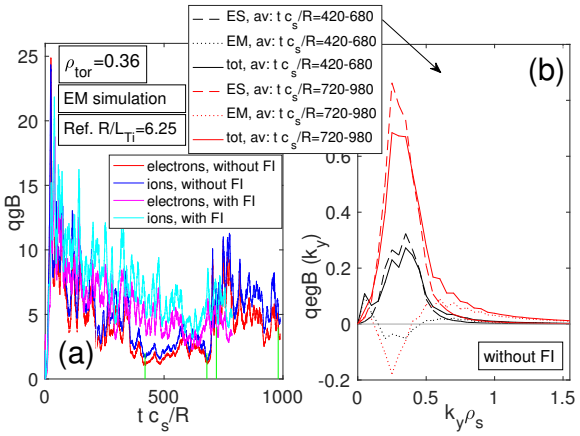

Figure 12. FI effect on NL fluxes at $\rho_{\rm tor} = 0.36$, with reference parameters. (a) The time traces of the NL fluxes in gyro-Bohm units from GENE EM simulations without FI (blue: ions, red: electrons) are compared with the ones including FI (cyan: ions, magenta: electrons). (b) Flux spectra from the two time intervals $t = 420 - 680\ R/c_s$ (black) and $t = 720 - 980\ R/c_s$ (red), indicated in green in (a).

strong that the fluxes are already very small and FI cannot further contribute to their stabilisation. It is interesting to note that in the simulation without FI (blue-red) there is a 'step-like' behaviour of the fluxes vs time. Looking at the average of the flux spectra over two consecutive steps (indicated by green vertical lines in Fig.12 (a)), which is shown in Fig.12 (b), it can be seen that in the 'smaller flux' phases a small EM peak at $k_y\rho_s = k_{y,min}\rho_s = 0.05$ is present, possibly suggesting an exchange of energy between low-k EM modes (compatible with the micro-tearings which have been observed in the linear regime, see section II) and smaller-scale ES modes (ITG). In the literature, different MTM-ITG nonlinear interaction regimes have been observed depending on parameters. There have been observations where MTM is linearly unstable, but shown to be nonlinearly suppressed when coinciding with ITG turbulence [54]. On the other hand, there are also regimes where nonlinear coupling to MTM is observed [15, 55]. Further analysis in this direction is beyond the scope of this work.

Coming back to the $\rho_{\rm tor} = 0.6$ case, for which the EM contribution to q_e has been retained, the origin of this EM part of the electron heat flux has been investigated in more detail. The portion of the EM contribution to the electron heat flux spectrum (dotted) coming from $B_{||}$ fluctuations has been separated (dash-dotted in the figure), and results to be $\simeq$ 6% of the EM flux. Thus the EM flux is almost totally coming from $B_\perp$ fluctuations. A convergence test has been performed for this case at $\rho_{\rm tor} = 0.6$, repeating part of the simulation with a finer grid. In particular, a larger y-box size L_y has been considered (corresponding to a smaller $k_{y,min} = 2\pi/L_y = 0.03/\rho_s$ wrt. standard $k_{y,min}\rho_s = 0.05$), setting $L_x = 200\rho_s \sim L_y$ in order to have $k_{x,min} \sim k_{y,min}$ and $n_{kx} \times n_{ky} \times n_z \times n_{v||} \times n_\mu = 256 \times 64 \times 32 \times 48 \times 15$ instead of the standard $n_{kx} \times n_{ky} \times n_z \times n_{v||} \times n_\mu = 128 \times 32 \times 32 \times 48 \times 15$ (see section II). The results of this test are shown in Fig.13.

The timetraces of $qigB$, $qegB$ are shown for the reference simulation (blue/red) and for the more resolved one (cyan/magenta). It can be seen that only the initial overshoot is modified in the latter, while after a slower decay it drops to similar values of the fluxes. It has to be noted that the initial overshoot in these simulations is very large, possibly enhanced by the initial phase, where the parallel flow shear is not balanced by the $E \times B$ shear until $t = 40R/c_s$ (indicated in the figure by a vertical line), while the zonal structures are still in development. Finally, an additional x-convergence test, where n_{kx} alone has been increased from 128 to 256, has been performed for the same case. The results, shown by dotted lines in Fig.13, indicate a much lower initial overshoot, followed by similar final values.

Turning to the GENE-QuaLiKiz benchmark, we shall come back to Fig.9. There is a good agreement on fluxes for the ES case (solid lines), while the QuaLiKiz EM mockup fails to reproduce the strong EM stabilisation (solid→dashed for GENE) at $\rho_{\rm tor} = 0.36$. However, the mockup correctly accounts for the upshift of the transport R/L_{Ti} threshold for the

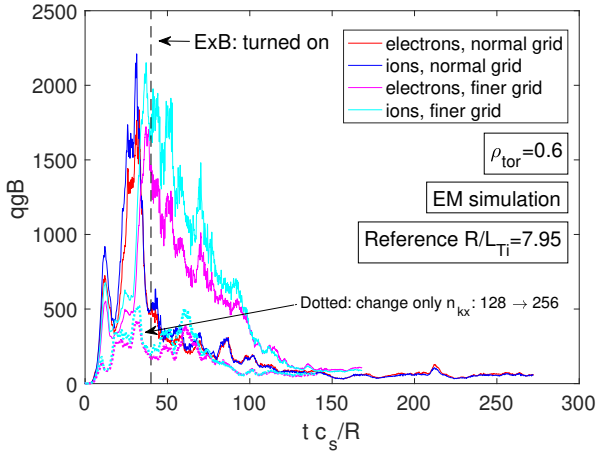

Figure 13. Time traces of the electron heat fluxes in gyro-Bohm units from the GENE NL EM simulation at $\rho_{\rm tor} = 0.6$ (corresponding to Fig.11 (b)), varying the grid resolution, as explained in the text. The lower resolution results are shown in blue (ions) and red (electrons), while the higher resolution ones are shown in cyan (ions) and magenta (electrons). The dotted lines correspond to an independent x-convergence test, where n_{kx} alone has been increased from 128 to 256.

same case. Since TGLF is able to model the linear EM stabilisation effects, its results are in better quantitative agreement with GENE at both radii. However, it still fails to account for the additional strong NL EM stabilisation at $\rho_{\rm tor} = 0.36$. At the same time, QuaLiKiz and TGLF are not able to account for both the lack of qgB vs R/L_{Ti} slope in GENE for the EM case and the fact that GENE predicts $q_e > q_i$ at $\rho_{\rm tor} = 0.6$ for the EM case.

B. Nonlinear deuterium-tritium comparison

The analysis of section IV A has been repeated considering a T plasma, i.e. keeping all the parameters constant except for the main ion mass and rescaling the $E \times B$ shearing rate according to what explained in section II, in order to evaluate the isotope effect on the heat transport. The results of the R/L_{Ti} scan of $qigB$ and $qegB$ at the two radii of analysis are shown in Fig.14.

Here, the ES and EM cases are illustrated in the first and second row, respectively, while the inner and outer radii in the first and second column, respectively.

Let's first consider the ES results, where QuaLiKiz and GENE are compared. GENE and QuaLiKiz agree on predicting a very small/negligible anti-gB effect at $\rho_{\rm tor} = 0.36$ ($1 \lesssim q(T)/q(D) = \sqrt{3/2}\, qgB(T)/qgB(D) \lesssim 1.2$ at reference R/L_{Ti}: $q(T)/q(D)$ is equal to $\sqrt{3/2} \sim 1.22$ for a pure gyro-Bohm scaling, it is ~ 1 for a mild anti-gB scaling with equal fluxes in physical units when changing isotope, while it becomes < 1 for a larger anti-gB scaling), while a larger but still small effect is seen at $\rho_{\rm tor} = 0.6$ ($0.8 \lesssim q(T)/q(D)[R/L_{Ti,ref.}] \lesssim 1$), for both ions and electrons. Turning to EM results, let's first consider the GENE-QuaLiKiz comparison. They also agree on predicting a very small/negligible anti-gB effect at $\rho_{\rm tor} = 0.36$ ($1.1 \lesssim q(T)/q(D)[R/L_{Ti,ref.}] \lesssim 1.2$), while they both predict a not small anti-gB effect at $\rho_{\rm tor} = 0.6$ ($0.4 \lesssim q(T)/q(D)[R/L_{Ti,ref.}] \lesssim 0.9$). It has to be noted that GENE is still completely lacking flux slope vs R/L_{Ti} also in T. Now, looking at TGLF results, even if the quantitative agreement on flux values with GENE is better than GENE-QuaLiKiz also in T, TGLF predicts a small anti-gB effect at both radii ($q(T)/q(D)[R/L_{Ti,ref.}] \sim 0.8$ at $\rho_{\rm tor} = 0.36$, $q(T)/q(D)[R/L_{Ti,ref.}] \sim 1.1$ at $\rho_{\rm tor} = 0.6$). However, the anti-gB effect is not negligible at $\rho_{\rm tor} = 0.36$ for TGLF, while it is negligible for GENE and QuaLiKiz. This could be due to the fact that the very strong nonlinear EM stabilisation which GENE sees at $\rho_{\rm tor} = 0.36$ somewhat hides/squeezes the anti-gB effect that could be expected for that case from linear results, which show smaller γ in T (see section II) wrt. D. On the contrary, TGLF could see this anti-gB effect since it underpredicts the EM stabilisation.

The gyro-Bohm scaling of the results can be better visualised looking at different plots, i.e. directly evaluating the ratio $q(T)/q(D)$ for ions and electrons. These plots, corresponding to the R/L_{Ti} scans of Fig.14, are here shown in Fig.15.

The same layout of Fig.14 is kept, i.e. ES/EM cases are indicated by different rows and the radii of analysis by different columns. Looking to these graphs, it is evident that the GENE/QuaLiKiz curves move down going from $\rho_{\rm tor} = 0.36$ to $\rho_{\rm tor} = 0.6$, leading to a non negligible anti-gB effect, at least in the EM case. TGLF, on the other hand, shows a small anti-gB effect at both radii. It thus seems that even if TGLF is in better agreement with GENE on the levels of the heat fluxes, QuaLiKiz gives a better estimate of the isotope dependence of the fluxes. However, this is a single example spanning a very narrow region of the possible parameter space which is compatible to hybrid cases of interest, therefore such a statement should be taken with caution and will need much more investigation with future benchmarks with GENE and other GK codes to be confirmed or confuted.

Finally, in order to identify the main responsibles of the observed anti-gB effect, some physics ingredients have been removed one by one by the reference GENE nonlinear simulations in D and T, and the output heat fluxes in gyro-Bohm units have been computed. The results of such analysis are shown in Fig.16 (a) and (b), corresponding to $\rho_{\rm tor} = 0.36$ and $\rho_{\rm tor} = 0.6$, respectively.

Starting from the case indicated as 'simple', corresponding to ES simulation with $s-\alpha$ geometry, without impurities, without FI, without rotation shear effects ($E \times B$ and parallel flow shear) in the collisionless regime, the single ingredients have been added one by one, eventually reaching the 'reference' cases of figures 14 and 15, as indicated. It results that the anti-gB effect is absent just for the ion channel in the 'simple' case. Then, 'pieces' of anti-gB effects are added up, still leading to a small effect, except from the EM case at $\rho_{\rm tor} = 0.6$. For that case, on the other hand, one has to note that the difference $qgB(D) - qgB(T)$ remains almost constant going from ES to EM case for both ions and electrons (the electron fluxes are almost unchanged, by the way), while the $q_i(T)/q_e(D)$ ratio lowers because the level of the ion fluxes decreases. Finally,

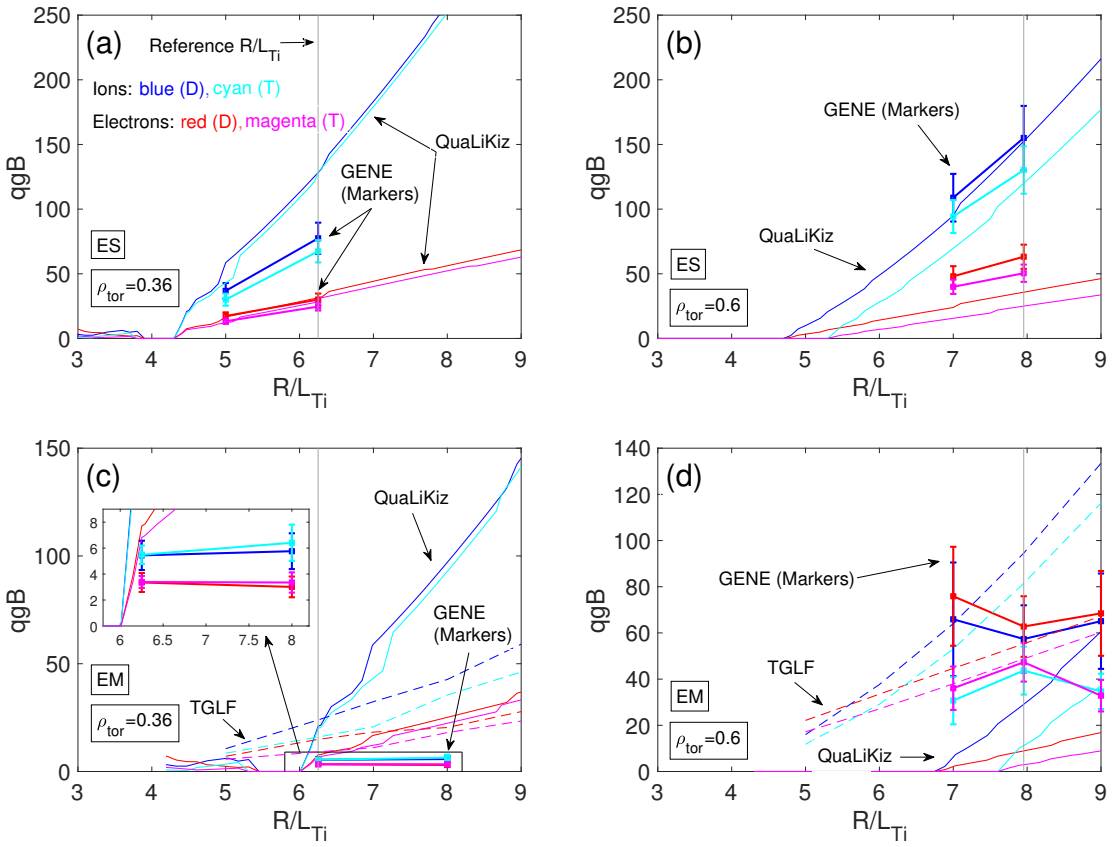

Figure 14. (color online) Isotope dependence of electron heat fluxes. GENE NL fluxes compared with QuaLiKiz and TGLF QL fluxes in gyro-Bohm units vs R/L_{Ti}, in D (blue and red correspond to ions and electrons, respectively) and T (cyan and magenta correspond to ions and electrons, respectively). The first and second row correspond to ES and EM simulations, respectively, while the first and second column to $\rho_{\rm tor} = 0.36$ and $\rho_{\rm tor} = 0.6$, respectively. GENE is distinguished by QuaLiKiz (both shown by solid lines) using square markers. TGLF is dashed.

one should note that the contributions coming from collisions and $E \times B$ shearing to the anti-gB effect are easily understood with respect to their dependence on normalization, as emphasized in the recent work [31]. Indeed, this paper indicates that, when keeping fixed the collision rates and the $E \times B$ shearing rate in ion units instead of physical units (as it is done in this work) when changing isotope, the related anti-gB effect should not show up. This means that once the dependence of qgB vs the collisional frequency (or vs the $E \times B$ shearing rate) in physical units is known for a considered isotope, the fluxes can be reconstructed for a second isotope just by rescaling the collisional frequency (or vs the $E \times B$ shearing rate) by the ratio of the square roots of the ion masses of the two isotopes. A preliminary test to investigate this behaviour has been made, repeating the reference EM GENE NL simulation at $\rho_{\rm tor} = 0.6$ in T, rescaling both γ_e and ν_c by $\sqrt{2/3}$ wrt. the values which have been used in this work. However, it seems that for this particular case the electron heat ion fluxes in T are almost unchanged ($\sim 2\%$ change) wrt. the ones obtained keeping the same rotation shear and collisions in physical units between the two isotopes, indicating a very small impact of rotation shear and collisions on these results and letting the anti-gB scaling almost unchanged, compared to the one of Fig.15 (d). Further analysis is then needed in the future to investigate this topic in view of the recent result of [31]. This would require repeating and investigating in more detail all the simulations in T, which is beyond the scope of this work.

V. CONCLUSIONS

A benchmark of the two quasi-linear models QuaLiKiz and TGLF by comparison with GK GENE ion-scale simulations has been performed considering parameters compatible with the high performance high β JET hybrid pulse 94875 in D. The parameters are taken from the end of a predictive JETTO simulation in D, where the fluxes were computed using QuaLiKiz neglecting ETGs. A detailed linear and nonlinear analysis has been carried out, repeating the simulations changing isotope from D to T in order to analyse the isotope effect. The GENE simulations retain all the most important physical effects, such as collisions, impurities, rotation shear effects, FI and EM effects and a realistic Miller geometry. The QL simulations have been set up to approximate at their best these effects, and the GENE simulations have been simplified to better compare with QL models when this was impossible.

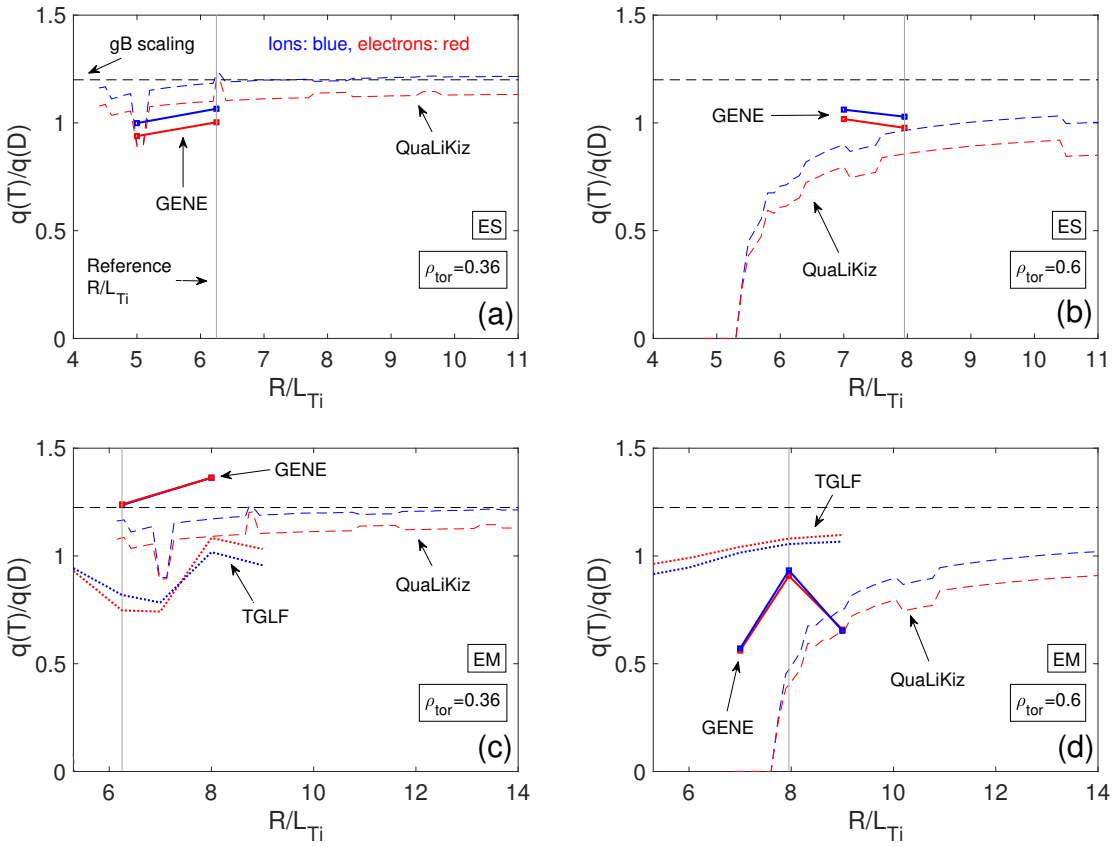

Figure 15. (color online) Ratio $q(T)/q(D) = \sqrt{3/2}\ qgB(T)/qgB(D)$ of the heat fluxes in physical units in T and D, vs R/L_{Ti}. GENE NL fluxes compared with QuaLiKiz and TGLF QL fluxes. Following Fig.14 layout, the first and second row correspond to ES and EM simulations, respectively, while the first and second column to $\rho_{\rm tor} = 0.36$ and $\rho_{\rm tor} = 0.6$, respectively. GENE is indicated by solid lines with square markers, while QuaLiKiz and TGLF by dashed and dotted lines, respectively. The horizontal dashed line indicates pure gB scaling, corresponding to $q(T)/q(D) = \sqrt{3/2} \sim 1.22$.

Linear analysis (section III):

- Spectra of the most unstable mode eigenvalues (ES and EM regimes): ITG-dominated ion-scales and ETG-dominated electron-scales;
- ETGs should not contribute to NL fluxes according to a linear criterion from [52];
- Strong EM stabilisation observed et $\rho_{\rm tor} = 0.36$, due to almost double β_e value compared to $\rho_{\rm tor} = 0.6$, together with a more efficient β_e stabilisation;
- Slightly smaller growth rates are found in T with respect to D at $\rho_{\rm tor} = 0.36$ in the EM regime;
- Both growth rate maxima and the corresponding k_y are found smaller for $s-\alpha$ geometry compared with Miller, in agreement with [51].
- QuaLiKiz-GENE comparison (only ES since QuaLiKiz is ES): qualitative agreement on the nature of micro-turbulence, quantitative agreement on eigenvalues only at the smaller k_y, which mostly contribute to the NL fluxes.
- TGLF-GENE comparison (both ES and EM): remarkably good agreement on both growth rates and frequencies;

NL analysis: simulations in D (section IV A):

- GENE heat fluxes in gyro-Bohm units vs R/L_{Ti} (main driver of ITG-dominated turbulence): very strong EM stabilisation at $\rho_{\rm tor} = 0.36$, even without FI, compared to $\rho_{\rm tor} = 0.6$, where a milder EM stabilisation is seen, almost only acting on ions;
- The GENE heat fluxes vs R/L_{Ti} have vanishing slope in the EM regime, and part of this 'flatness' is explained by an enhanced linear β_e stabilisation at larger R/L_{Ti};
- QuaLiKiz-GENE comparison (ES and EM with QuaLiKiz mockup): good agreement in the ES regime, but QuaLiKiz is not able to capture the EM stabilisation at $\rho_{\rm tor} = 0.36$, even using its EM mockup. Nevertheless, the mockup is able to correctly estimate the heat transport R/L_{Ti} threshold shift going from ES to EM case;
- TGLF-GENE comparison (only EM): better agreement than QuaLiKiz-GENE on flux levels, since TGLF is

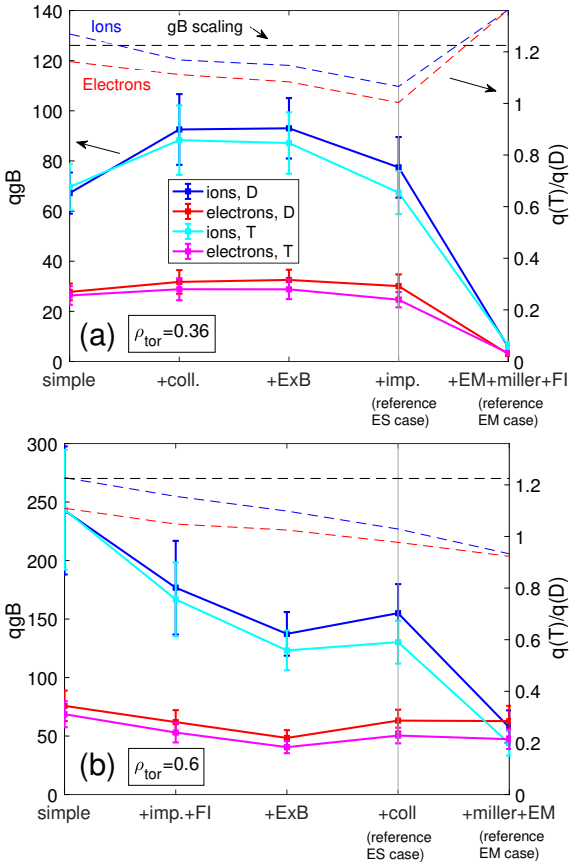

Figure 16. (color online) Isotope dependence of electron heat fluxes at $\rho_{tor} = 0.36$ (a) and $\rho_{tor} = 0.6$ (b), for reference R/L_{Ti} values, adding physics ingredients starting from a 'simple' case, corresponding to ES simulation with $s - \alpha$ geometry, without impurities, without FI, without rotation shear effects ($E \times B$ and parallel flow shear) in the collisionless regime. GENE NL fluxes are compared with QuaLiKiz and TGLF QL fluxes in gyro-Bohm units (left y-axis), in D (blue and red correspond to ions and electrons, respectively) and T (cyan and magenta correspond to ions and electrons, respectively). The ratio $q(T)/q(D) = \sqrt{3/2}\ qgB(T)/qgB(D)$ of the heat fluxes in physical units in T and D has been added to the figure (right y-axis), following Fig.15, for ions (blue dashed line) and electrons (red dashed line). The horizontal dashed line indicates pure gB scaling, corresponding to $q(T)/q(D) = \sqrt{3/2} \sim 1.22$.

able to model the linear EM stabilisation. However, because it lacks NL EM stabilisation physics, TGLF does not fully account for the strong EM stabilisation at the inner radius;

- Both QuaLiKiz and TGLF: do not agree with GENE on the vanishing heat fluxes slope vs R/L_{Ti} for the EM cases at both radii and they are not able to reproduce the $q_e > q_i$ condition that holds for GENE simulations at $\rho_{tor} = 0.6$ for the EM case, due to a positive EM contribution coming to q_e from perpendicular magnetic field fluctuations.

NL analysis: D-T comparison: the simulations of section IV A have been repeated in T (section IV B):

- GENE and QuaLiKiz: agree on predicting a negligible anti-gB effect at $\rho_{tor} = 0.36$, which increases with increasing radius and is not small at $\rho_{tor} = 0.6$ for the EM case;
- TGLF: small anti-gB effect at both radii;
- GENE: gB behaviour only appears for the ion channel when removing physics ingredients such as impurities, collisions, FI, rotation shear effects ($E \times B$ and parallel flow shear) and shaping (physics ingredients such as collisions, impurities, FI, rotation shear have been removed in GENE NL simulations one by one from the reference cases to single out the main contributions to the observed anti-gB effect).

Coming back to the main focus of this paper, i.e. the benchmark of quasi-linear models with GK, the outcome is that even if TGLF gives best estimates of the absolute level of the heat fluxes compared to GENE, QuaLiKiz compares better to GENE regarding the estimate of the relative isotope dependence of the fluxes for the considered case. This will need further analysis in the future, spanning larger parameter regions which are compatible with hybrid cases of interest, also comparing QL and GK results with experiments. Finally, the upcoming JET campaign in T will allow to compare experimental measurements with our predictions.

ACKNOWLEDGEMENTS

This work has been carried out within the framework of the EUROfusion Consortium and has received funding from the Euratom research and training programme 2014-2018 and 2019-2020 under grant agreement number 633053. The views and opinions expressed herein do not necessarily reflect those of the European Commission. The numerical simulations have been carried out on the MARCONI cluster at CINECA.

REFERENCES

[1] Brizard A.J., and Hahm T.S. 2007 *Rev. Mod. Phys.* **79** 421
[2] Bourdelle C., Garbet X., Imbeaux F., Casati A., Dubuit N., Guirlet R., and Parisot T., 2007 *Phys. Plasmas* **14** 112501
[3] Citrin J., Bourdelle C., Casson F.J., Angioni C., Bonanomi N., Camenen Y., Garbet X., Garzotti L., Görler T., Gürcan O. *et al.* 2017 *Plasma Phys. Control. Fusion* **59**

[4] Staebler G.M., Kinsey J.E., and Waltz R.E., 2007 *Phys. Plasmas* **14** 055909

[5] Staebler G.M., Candy J., Howard N.T. and Holland C. 2016 *Phys. Plasmas* **23** 062518

[6] Mantica P., Angioni C., Bonanomi N. , Citrin J., Grierson B.A., Koechl F., Mariani A., Staebler G.M. *et al.* 2020 *Plasma Phys. Control. Fusion* **62** 014021

[7] Grierson B.A., Staebler G.M., Solomon W.M., McKee G.R., Holland C., Austin M., Marinoni A., Schmitz L., Pinsker R.I. *et al.* 2018 *Phys. Plasmas* **25** 022509

[8] Koechl F. *et al.* 2018 Proc. 27th IAEA FEC IAEA CN-258, EX/P7-25

[9] Bonanomi N., Mantica P., Citrin J., Giroud C., Lerche E., Sozzi C., Taylor D., Tsalas M., Van Eester D. *et al.* 2018 *Nucl. Fusion* **58** 026028

[10] Mantica P. 2016 Invited Talk at 58th APS DPP Meeting, S Jose, CA

[11] Mantica P. *et al.* 2018 Poster at 23rd EU-US Transport Task Force Meeting, Sevilla, ES

[12] Bonanomi N., Casiraghi I., Mantica P., Challis C., Delabie E., Fable E., Gallart D., Giroud C., Lerche E., Lomas P. *et al.* 2019 *Nucl. Fusion* **59** 096030

[13] Casson F.J., Patten H., Bourdelle C., Breton S., Citrin J., Koechl F., Sertoli M., Angioni C., Baranov Y., Bilato R. *et al.* 2020 *Nucl. Fusion* **60** 066029

[14] Staebler G.M. 2018 *Nucl. Fusion* **58** 115001

[15] Citrin J., Garcia J., Görler T., Jenko F., Mantica P., Told D., Bourdelle C., Hatch D.R., Hogeweij G.M.D., Johnson T. *et al.* 2015 *Plasma Phys. Control. Fusion* **57** 014032

[16] Citrin J., Jenko F., Mantica P., Told D., Bourdelle C., Garcia J., Haverkort J.W., Hogeweij G.M.D., Johnson T., and Pueschel M.J. 2013 *Phys. Rev. Lett.* **111** 155001

[17] Garcia J., Challis C., Citrin J., Doerk H., Giruzzi G., Görler T., Jenko F., Maget P. *et al.* 2015 *Nucl. Fusion* **55** 053007

[18] Di Siena A., Görler T., Poli E., Bañón Navarro A., Biancalani A., and Jenko F. 2019 *Nucl. Fusion* **59** 124001

[19] Whelan G.G., Pueschel M.J., and Terry P.W. 2018 *Phys. Rev. Lett.* **120** 175002

[20] Bessenrodt-Weberpals M., Wagner F., Gehre O., Giannone L., Hofmann J.V., Kallenbach A., McCormick K., Mertens V., Murmann H.D., Ryter F. *et al.* 1993 *Nucl. Fusion* **33** 1205

[21] Barnes C.W., Scott S.D., Bell M.G., Bell R., Budny R.V., Bush C.E., Fredrickson E.D., Grek B., Hill K.W., Janos A. *et al.* 1996 *Phys. Plasmas* **3** 4521

[22] Maggi C.F., Weisen H., Hillesheim J.C., Chankin A., Delabie E., Horvath L., Auriemma F., Carvalho I.S., Corrigan G., Flanagan J. *et al.* 2018 *Plasma Phys. Control. Fusion* **60** 014045

[23] Schneider P.A., Bustos A., Hennequin P., Ryter F., Bernert M., Cavedon M., Dunne M.G., Fischer R., Görler T., Happel T. *et al.* 2017 *Nucl. Fusion* **57** 066003

[24] E. Joffrin, S. Abduallev, M. Abhangi, P. Abreu, V. Afanasev, M. Afzal, K.M. Aggarwal, T. Ahlgren, L. Aho-Mantila, N. Aiba *et al.* 2019 *Nucl. Fusion* **59** 112021

[25] J. Garcia, R.J. Dumont, J. Joly, J. Morales, L. Garzotti, T.W. Bache, Y. Baranov, F.J. Casson, C. Challis, K. Kirov *et al.* 2019 *Nucl. Fusion* **59** 086047

[26] Oberparleiter M. *et al.* 2018 Poster at 23rd EU-US Transport Task Force Meeting, Sevilla, ES

[27] Schneider P.A. et al., "Fast-ion pressure dominating the mass dependence of the core heat transport in ASDEX Upgrade H-modes" submitted to *Nucl. Fusion*

[28] Schneider P.A. et al., "Overview of the isotope effects in the ASDEX Upgrade tokamak", special issue on PPCF, in preparation

[29] Garcia J., Görler T., and Jenko F. 2018 *Phys. Plasmas* **25** 055902

[30] Scott B.D. 1992 *Phys. Fluids B* **4** 2468

[31] Belli E. A., Candy J., and Waltz R.E. 2020 *Phys. Rev. Lett.* **125**, 015001

[32] Nakata M., Nunami M., Sugama H., and Watanabe T.H. 2017 *Phys. Rev. Lett.* **118** 165002

[33] Garcia J., Görler T., Jenko F., and Giruzzi G. 2017 *Nucl. Fusion* **57** 014007

[34] Manas P., Angioni C., Kappatou A., Ryter F., Schneider P.A. *et al.* 2019 *Nucl. Fusion* **59** 014002

[35] Garbet X. and Waltz R.E. 1996 *Phys. Plasmas* **3** 1898

[36] Maggi C.F., Weisen H., Casson F.J., Auriemma F., Lorenzini R., Nordman H., Delabie E., Eriksson F., Flanagan J., Keeling D. *et al.* 2019 *Nucl. Fusion* **59** 076028

[37] H. Dudding, *private communication*

[38] Jenko F., Dorland W., Kotschenreuther M. and Rogers B.N. 2000 *Phys. Plasmas* **7** 1904

[39] Görler T., Lapillonne X., Brunner S., Dannert T., Jenko F., Merz F., and Told D. 2011 *J. Comput. Phys.* **230** 7053

[40] Romanelli M., Corrigan G., Parail V., Wiesen S., Ambrosino R., Da Silva Aresta Belo P., Garzotti L., Harting D., Köchl F., Koskela T. *et al.* 2014 *Plasma Fusion Res.* **9** 3403023

[41] Citrin J. *et al.*, to be submitted to *Nucl. Fusion*

[42] Lao L.L., St. John H., Stambaugh R.D., and Pfeiffer W. 1985 *Nucl. Fusion* **25** 1421

[43] Brix M., Hawkes N.C., Boboc A., Drozdov V., Sharapov S. E. *et al.* 2008 *Rev. Sci. Instrum.* **79** 10F325

[44] Sauter O. 2016, *Fusion Eng. Des.* **112** 633

[45] Miller R.L., Chu M.S., Greene J.M., Lin-Liu Y.R., and Waltz R.E. 1998 *Phys. Plasmas* **5** 973

[46] Connor J.W., Hastie R.J., and Taylor J.B. 1978 *Phys. Rev. Lett.* **40** 396

[47] G. M. Staebler, J. Candy, E. A. Belli, J. E. Kinsey, N. Bonanomi and B. Patel 2021 *Plasma Phys. Control. Fusion* **63** 015013

[48] Staebler G.M., Kinsey J.E., and Waltz R.E. 2007 *Phys. Plasmas* **14** 055909

[49] Zonca F., Chen L., and Santoro R.A. 1996 *Plasma Phys. Control. Fusion* **38** 2011

[50] Terry P.W., Carmody D., Doerk H., Guttenfelder W., Hatch D.R., Hegna C.C., Ishizawa A., Jenko F., Nevins W.M., Predebon I. *et al.* 2015 *Nucl. Fusion* **55** 104011

[51] Lapillonne X., Brunner S., Dannert T., Jolliet S., Marinoni A., Villard L., Görler T., Jenko F., and Merz F. 2009 *Phys. Plasmas* **16** 032308

[52] Staebler G.M., Howard N.T., Candy J., and Holland C. 2017 *Nucl. Fusion* **57** 066046

[53] F. Jenko, W. Dorland and G.W. Hammett 2001 *Phys. Plasmas* **8**, 4096.

[54] H. Doerk, M. Dunne, F. Jenko, F. Ryter, P.A. Schneider, E. Wolfrum, and The ASDEX Upgrade Team 2015 *Phys. Plasmas* **22**, 042503

[55] D.R. Hatch, M.J. Pueschel, F. Jenko, W.M. Nevins, P.W. Terry, and H. Doerk 2012 *Phys. Rev. Lett.* **108** 235002